Quantitative determination of charge transfer parameters of photorefractive $BaTiO_3$:Rh from EPR-based defect studies

2003 J. Phys.: Condens. Matter 15 415

(http://iopscience.iop.org/0953-8984/15/3/307)

INSTITUTE OF PHYSICS PUBLISHING JOURNAL OF PHYSICS: CONDENSED MATTER

J. Phys.: Condens. Matter **15** (2003) 415–429 PII: S0953-8984(03)53314-8

Quantitative determination of charge transfer parameters of photorefractive $BaTiO_3$:Rh from EPR-based defect studies

C Veber[1], M Meyer[1], O F Schirmer[1] and M Kaczmarek[2]

[1] Fachbereich Physik, Universität Osnabrück, D-49069 Osnabrück, Germany
[2] Department of Physics and Astronomy, University of Southampton, Southampton S017 1BJ, UK

E-mail: schirmer@uos.de

Received 29 August 2002
Published 13 January 2003
Online at stacks.iop.org/JPhysCM/15/415

Abstract

Optical absorption bands can be used as fingerprints of defects and their charge states in insulators and semiconductors. On the basis of the photochromicity usually shown by such materials, a method is introduced by which the optical bands are assigned to the defects and their charge states. It is based on simultaneous measurements of the light-induced changes of the optical absorption and of the corresponding EPR signals. Moreover, indirectly optical bands of EPR-silent defects can also be labelled in this way, strongly widening the scope of EPR based defect studies. We apply this method to the infrared-sensitive photorefractive system $BaTiO_3$:Rh, where illumination leads to recharging among the valence states Rh^{5+}, Rh^{4+} and Rh^{3+}. The values of all parameters governing the charge transfers responsible are inferred from the magnitude of the absorption bands, the absolute determination of their absorption cross-sections and the kinetics of the absorption changes under illumination. In contrast to previous investigations, these parameters are deduced independently of photorefractive measurements.

(Some figures in this article are in colour only in the electronic version)

1. Introduction

Under excitation by suitable illumination many insulators and semiconductors that contain defects show light-induced absorption changes, i.e. they are photochromic. This feature is also observed in most inorganic photorefractive materials. It is caused by photo-induced charge transfers between the defects, often leading to metastable charge rearrangements stabilized by lattice distortions. Since the optical absorption of defects depends on their charge states, any changes of the valences will lead to optical absorption changes. Photochromicity is, of course,

particularly relevant at low temperatures; however, depending on the specific material and the defects it contains, light-induced colouration may also persist at room temperature. We have shown [1, 2] that this phenomenon can be used for correlating EPR spectra of defects with their absorption spectra. In a convenient way it allows us to monitor the changes of EPR and optical signals simultaneously. Parallel variations in both quantities indicate that both EPR and optical absorption may result from the same microscopic origin. In this way, the information about the identity of the defects and their structures, derived from the analysis of the EPR spectra, can be used to interpret the optical signals. These can then serve to indicate the presence of the corresponding defects in the material. It is thus possible to use the optical bands as fingerprints for the defects instead of their EPR spectra. This often offers the advantage that defects can be identified also at room temperature, whereas EPR studies alone have to be performed in most cases at low temperatures.

The procedure is not restricted, however, to the identification of EPR-active defects via their optical bands. Light-induced absorption changes can be introduced by two or more defects that are related to each other by electron interchange under illumination. On the basis of the established optical fingerprints of EPR-active defects, a self-consistent interpretation of the accompanying photochromic changes can then also assign EPR-silent defects to their optical bands. Examples of this procedure will be given below. The possibility of obtaining optical fingerprints of EPR-silent defects is a particularly valuable feature of the combined EPR–optical absorption method.

Defects and the light-induced charge transfer processes between them play an essential role in photorefractive crystals. Illumination by an inhomogeneous light pattern photoionizes defects and creates quasi-free charge carriers. They are transported out of the illuminated regions by various charge driving mechanisms, among them diffusion, and tend to settle in the darker regions of the sample. This creates a space charge field, which is transformed into a refractive index pattern in materials with a non-zero electrooptic effect. It is evident that a thorough knowledge of the structure and properties of the defects involved in these processes is necessary in order to steer and improve the operation of photorefractive crystals.

In previously published work, we applied the combined EPR–optical absorption procedure to a series of photorefractive materials [3, 4], qualitatively unravelling the responsible light-induced charge transfer paths taking place under homogeneous illumination. In this paper, we show how to determine the parameters governing light-induced charge transfer processes quantitatively. In particular we demonstrate that photorefractive properties of a material can be predicted just from the charge transfer behaviour of the defects, as based on EPR studies. Previously, on the basis of optical studies alone, it had been difficult to obtain this essential information. Relying solely on optical and, in particular, photorefractive measurements, bands were sometimes inconclusively assigned to their microscopic origins or the charge transfer parameters had to be deduced from oversimplified models.

The system treated here as an example is $BaTiO_3$ doped with Rh. The electrooptic tensor of the host lattice contains rather large coefficients, and thus even relatively few transposed charges are sufficient to create measurable index changes. Moreover, doping with Rh is known to improve the infrared sensitivity of the material [5–9].

2. Method

Figure 1 shows the three elementary schemes describing light-induced charge transfer in crystals [10]. More complicated cases are also possible, consisting of a combination of these schemes. In the examples presented in figure 1, the primary processes, symbolized by double arrows, are assumed to consist of electron excitations from the valence band to the defect

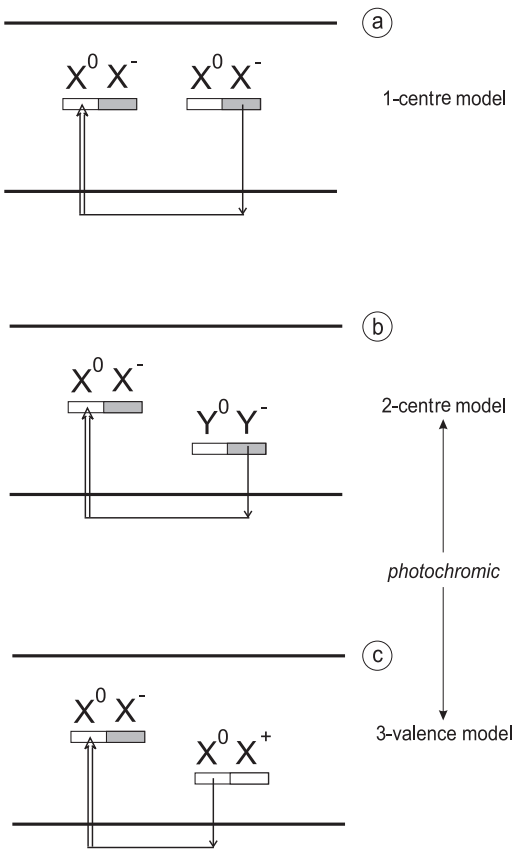

Figure 1. The three basic schemes for band charge transfer processes between defect gap levels. The lower two lead to light-induced optical absorption under homogeneous illumination. The graphs show an example of hole conduction, as found for $BaTiO_3$:Rh.

levels. This can also be viewed as hole photoionization. Alternatively—and not shown here—photorefractive processes can be dominated by electron transfer from defects to the conduction band. Single arrows in figure 1 depict secondary processes; they are triggered by the primary ones, for instance involving capturing of ionized charges at spatially separated defects. In all cases the arrows indicate the direction of the electron flow. In figure 1(a) the photoionized holes are trapped at the same defect type from which they originated, constituting the 'one-centre model'. In figure 1(b) (the 'two-centre model') two different defect species, the deep X and the shallow Y, are involved; in figure 1(c) (the 'three-valence model') three different charge states of the same defect occur. In the two lower cases of figure 1, the final defect levels differ from the original ones and that leads to the photochromic effect. This means that in these cases homogeneous illumination can already cause light-induced absorption changes, whereas the scheme in figure 1(a) is sensitive only to inhomogeneous illumination. While the 'one-centre model' can be valid at room temperature, it is not expected to be fulfilled at low temperatures, where shallow intermediate levels, such as those in figure 1(b), tend to capture the photoionized carriers for extended periods of time. Thus photochromicity, the basis for the application of our method, is present in all cases and should be particularly relevant at lower temperatures.

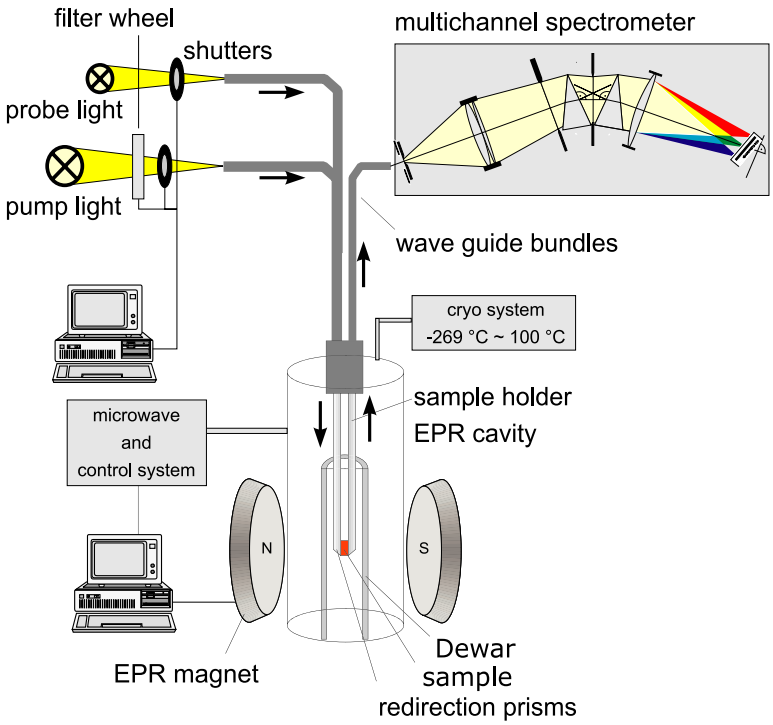

Figure 2. Set-up for the combined EPR–optical absorption investigations of light-induced signal changes. The crystal sample, centred in the EPR cavity between two half-cylindrical quartz rods, is first illuminated by intense monochromatic pump light for typically 60 s; the resulting signal changes are then simultaneously probed by EPR and weak, 20 ms pulsed white probe light with an energy range covering about 1–3 eV. The transmitted light, guided by prisms at the ends of the quartz rods, is dispersed by a double prism spectrometer and registered with a multichannel detector.

The light-induced absorption changes are measured with a specially developed set-up (figure 2) [1]. Its pump light source consists of a xenon arc lamp and a set of 17 interference filters to narrow the bandwidth of the beam. Light is typically applied for 1 min. At room temperature this drives the absorption changes into saturation. After this step, the absorption state of the photochromic crystal is monitored by weak, wideband probe light for a duration of usually 20 ms. This probe light, taking the same path as the pump light, is transmitted through the sample, then dispersed by a double prism, and all wavelengths are simultaneously detected by a 1024 diode array detector. The crystal specimen itself is held in an EPR cavity between two half-cylindrical quartz glass rods. Flexible light guides connect the rods to the light sources and the spectrometer. This set-up allows simultaneous optical and EPR measurements in a rather versatile way.

Figures 3(a) and (b) demonstrate the spectra of absorption changes, observed with an 'as-grown' $BaTiO_3$ crystal, containing Rh as unintended defects. After each of the successive illuminations with one of the 17 pump energies (indicated by horizontal bars along the ordinate in figure 3(a)), starting at low energies, the absorption changes are monitored. The raw data, as plotted in figure 3(b), look rather complex; more insight into the systematic structure of these results can be obtained if they are plotted in a pseudo-3D way, as in figure 3(a). While the abscissa is given by the probe light energy, E_{probe}, as in figure 3(b), the ordinate is equivalent

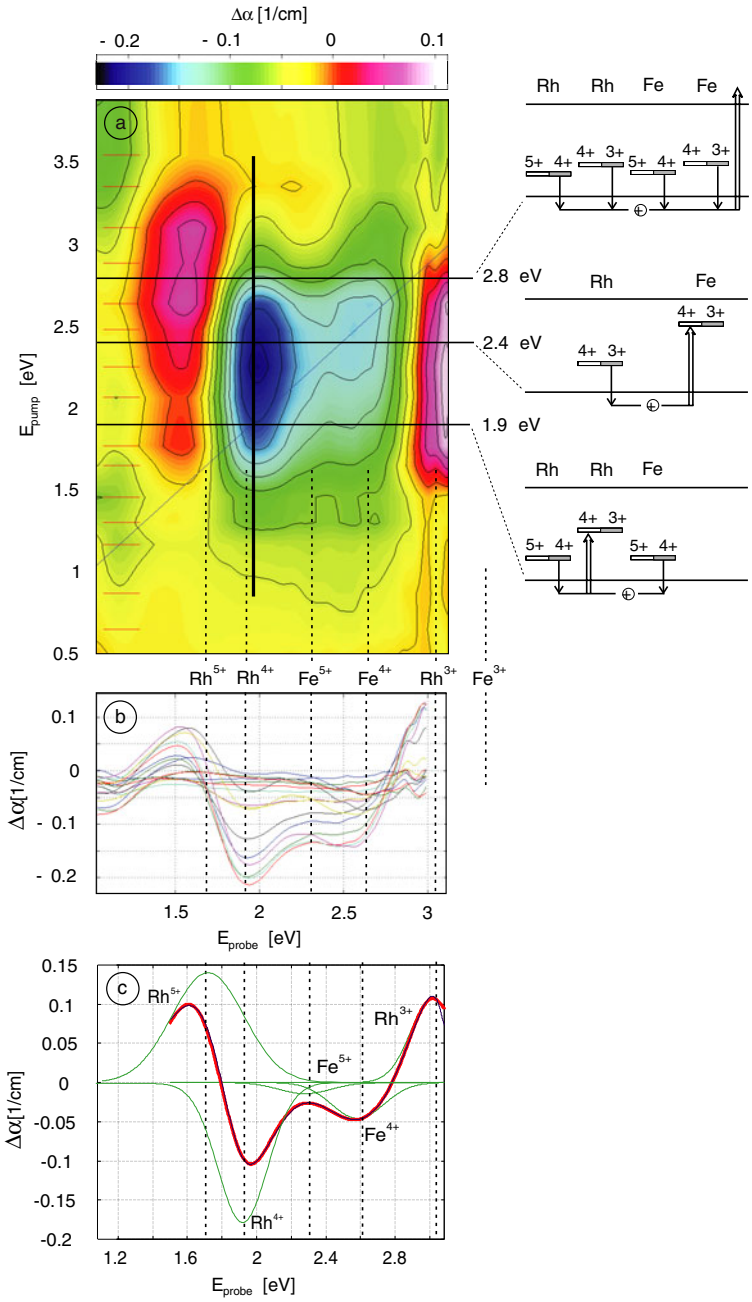

Figure 3. (a) Pseudo-3D plot of optical absorption changes in $BaTiO_3$:Rh after sequential illumination with 17 different pump energies. Abscissa: probe light energy. Ordinate: pump light energy. Colour code: absorption changes, as calibrated by the bar on top. Separation of the total absorption changes into Gaussian component bands leads to the assignment to the various charge states of Rh and Fe, as indicated by the broken lines. The variation of the plot under different pumping energies is analysed at the right by the appropriate level schemes. (b) Raw data for the plot in figure 3(a): series of absorption changes, each taken after illumination with the sequence of 17 pump energies. (c) Light-induced absorption change after pumping at 1.9 eV and separation into its component Gaussian bands.

to the pump energy, E_{pump}. The magnitude of the absorption changes is represented by the colour code, as calibrated by the upper horizontal bar.

The continuity of the plot is obtained from numerical linear interpolation of the discrete changes in absorption spectra taken at the 17 pump energies, figure 3(b). An important guideline is the diagonal in figure 3(a), where $E_{probe} = E_{pump}$. Along this line the primary charge transfer processes occur, which trigger the photochromic effect. Pumping into these transitions causes the initial charge of the defect to be reduced and this in turn tends to exhaust the number of ions available for the respective transition. As a result, the strength of the responsible absorption band, monitored by E_{probe}, is decreased. We thus observe that light-induced transparencies occur along the diagonal line and this is a typical consequence of primary processes. Secondary processes are usually lying outside of the diagonal. It should be noted that all the absorption changes in figure 3 are dominated by charge transfer processes. Alternative processes, such as crystal field d–d transitions, are essentially parity-forbidden and are thus much weaker. These are therefore not considered in our arguments.

As will become evident from the further discussion, the plots, such as those in figure 3, contain a lot of information on the charge transfer behaviour of a specific crystal. Experience with such measurements shows that hardly any two identically doped samples, sometimes even if cut from the same boule, lead to identical absorption maps of the type of figure 3(a). The method thus constitutes a rather convenient technique to characterize individual specimens with respect to their impurity content and behaviour.

3. Results

3.1. Qualitative aspects

There are three main features in figure 3(a): the strong light-induced transparency near $E_{probe} = 1.9$ eV and pronounced absorption increases near 1.6 and 3.0 eV. In our previous work we established a correlation between the decreasing absorption near 1.9 eV and the EPR spectrum of Rh^{4+} [11]; both signal types vary in the same way with changing energy, E_{pump}, and for constant $E_{probe} = 1.9$ eV, i.e. along the corresponding vertical line in figure 3(a). The absorption band at 1.9 eV was thus attributed to a transfer of a valence band electron to Rh^{4+}, creating Rh^{3+}. In this process a hole remains in the valence band. It was furthermore shown [12], that capture of this hole at another Rh^{4+} defect, forming Rh^{5+}, leads to the increase near 1.6 eV. It is then straightforward to attribute the strong absorption rise near 3.0 eV to Rh^{3+}, since it is correlated to the increase of Rh^{5+} and anticorrelated to the decrease of Rh^{4+}. All these changes apparently fulfil the three-valence model, figure 1(c), according to reaction 2, $Rh^{4+} \rightarrow Rh^{3+} + Rh^{5+}$. It is worthwhile mentioning that only Rh^{4+} is EPR-active [13]. By assigning the other bands to Rh^{5+} and Rh^{3+}, these EPR-silent charge states can now be detected by their 'optical fingerprints'.

Along the diagonal in figure 3(a), further features appear which cannot be attributed to any of the Rh charge states. The slight transparency along the diagonal near 2.6 eV is due to charge transfer transitions to Fe^{4+} [14], whereas the feature near 2.3 eV is caused by Fe^{5+} [14, 15]. In this way the entire 'landscape' in figure 3(a) can be analysed in terms of the five components mentioned, namely Rh^{3+}, Rh^{4+}, Rh^{5+}, Fe^{4+} and Fe^{5+}. Assuming that the corresponding optical bands have Gaussian shapes, the absorption change occurring after pumping with 1.9 eV is decomposed into its component bands as shown in figure 3(c). It is observed that the peak energies of the component bands can differ considerably from the energies of the extrema of the total absorption changes. All in all, it can be seen that the main reaction induced by pumping with 1.9 eV light obeys the three-valence model, as indicated

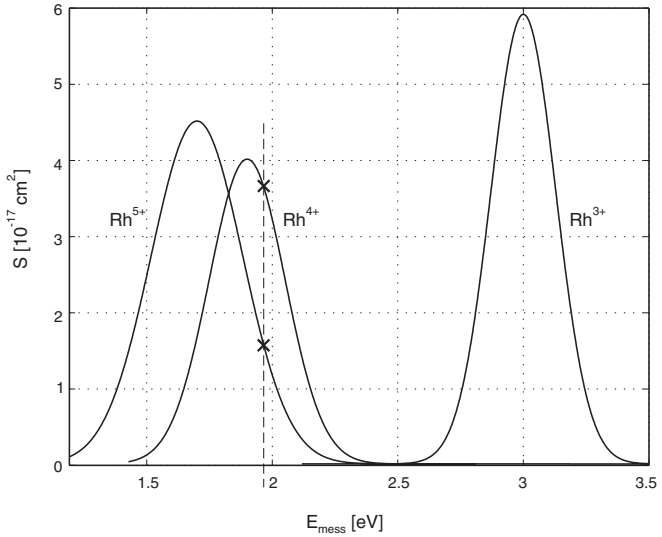

Figure 4. Energy dependence of the optical absorption cross-sections of the three Rh charge states involved. The values of $S(Rh^{4+})$ and $S(Rh^{5+})$, active at 1.96 eV—the pump light energy used in the time dependence of the absorption changes (figure 6)—are indicated by x.

above: 2 $Rh^{4+} \rightarrow Rh^{3+} + Rh^{5+}$. Superimposed are weak charge transfers to Fe^{4+} and Fe^{5+}. Of course, by changing the pump energy, new primary processes will be activated. At the right side of figure 3(a) such different primary processes and their secondary consequences are indicated in the respective band diagrams.

In assessing the level structure at the right of figure 3(a) it is seen that levels defined by the same defect charge pair, e.g. $Rh^{3+/4+}$, can occur with two different energy distances to the valence band edge. Here it is worth noting that optical levels have to be distinguished from thermal ones. The former are reached by primary transitions under Franck–Condon conditions, whereas the latter are connected to the valence band by secondary transitions.

3.2. Quantitative analysis

We base this analysis on the fact that band intensities are proportional to the densities of the related defects. For the case of the EPR-active Rh^{4+}, we determine the factor of proportionality by comparing the EPR signal with that of a standard containing a known number of spins. A small crystal of $CuSO_4{\cdot}5H_2O$ was used for this purpose, each molecule containing one unpaired spin, $S = 1/2$. Proceeding with the evaluation as described, e.g., by Weil *et al* [16], it is found that the $BaTiO_3$:Rh sample contains $N(Rh^{4+}) = 1.0 \times 10^{17}$ cm^{-3} Rh^{4+} ions. Comparing this density with the light-induced absorption change $\Delta\alpha$ of the Rh^{4+} band, the absorption cross-section S of Rh^{4+} is determined according to the relation $\Delta\alpha(Rh^{4+}) = \Delta N(Rh^{4+}) \cdot S(Rh^{4+})$. The result is shown in figure 4. Assuming the validity of the three-valence model, 2 $Rh^{4+} \rightarrow Rh^{3+} + Rh^{5+}$, the decrease, $\Delta N(Rh^{4+})$, is accompanied by the increases, $\Delta N(Rh^{3+}) = \Delta N(Rh^{5+}) = -1/2\Delta N(Rh^{4+})$. In using this relation we neglect the weak changes of the Fe^{4+} and Fe^{5+} concentrations and we can then infer the absorption cross-sections of Rh^{3+} and Rh^{5+} (figure 4). Knowing these quantities, the initial concentrations of the respective Rh ions in the crystal before illumination are determined by separating the total absorption of the crystal into its component bands. Table 1 shows the resulting concentrations

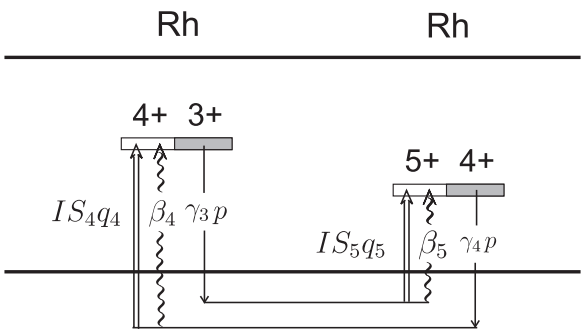

$$\begin{aligned}
\dot{Rh}^{3+} &= (IS_4q_4 + \beta_4)\, Rh^{4+} - \gamma_3\, p\, Rh^{3+} \\
\dot{Rh}^{5+} &= -\ (IS_5q_5 + \beta_5)\, Rh^{5+} + \gamma_4\, p\, Rh^{4+} \\
\dot{Rh}^{4+} &= -\dot{Rh}^{3+} - \dot{Rh}^{5+}
\end{aligned}$$

Figure 5. Three-valence model together with the rate equations governing the recharging of the Rh levels following thermal (wavy arrows) and optically (double arrows) induced transfer processes. The level positions are given schematically; optical and thermal levels are not distinguished. For simplicity it is not indicated that thermal transitions always originate from the band edge, while optical transitions may also start from the depth of the band.

Table 1. Parameters describing charge transfer processes in $BaTiO_3$ involving Rh charge states. (For the energy dependence of the S_i see figure 4.)

Generally valid parameters	
q_4	0.01 ± 0.01
q_5	1
β_4	$(1.4 \pm 0.5) \times 10^{-2}$ s^{-1}
β_5	(1.4 ± 0.7) s^{-1}
γ_3	$(1.4 \pm 0.5) \times 10^{-13}$ cm^3 s^{-1}
γ_4	$(2.7 \pm 0.7) \times 10^{-12}$ cm^3 s^{-1}
$S_{3,max}$	$(6.0 \pm 2.4) \times 10^{-17}$ cm^2
$S_{4,max}$	$(4.0 \pm 2.0) \times 10^{-17}$ cm^2
$S_{5,max}$	$(4.5 \pm 2.0) \times 10^{-17}$ cm^2
Parameters characteristic for the investigated crystal	
Initial Rh concentrations:	
Rh^{4+}	$(1.0 \pm 0.5) \times 10^{17}$ cm^{-3}
Rh^{3+}	$(4.0 \pm 2.2) \times 10^{17}$ cm^{-3}
Rh^{5+}	$(0.5 \pm 0.3) \times 10^{17}$ cm^{-3}
Rh_T	$(5.5 \pm 3.0)\ 10^{17}$ cm^{-3}
	(equiv. to about (40 ± 20) ppm)
Hole density (typical value):	
p	$(0.7 \pm 0.5) \times 10^{10}$ cm^{-3}

of the three Rh valences and their absorption cross-sections. The quality of the decomposition of the total absorption change into its components is indicated by the fact that $\Delta\alpha$ (measured)—$\Delta\alpha$ (reconstructed) in the plane of figure 3(a) is nowhere larger than 10^{-3} cm^{-1}.

One important advantage of the present method is that information on the concentrations of the individual defects involved in the charge transfer processes can be derived from the EPR

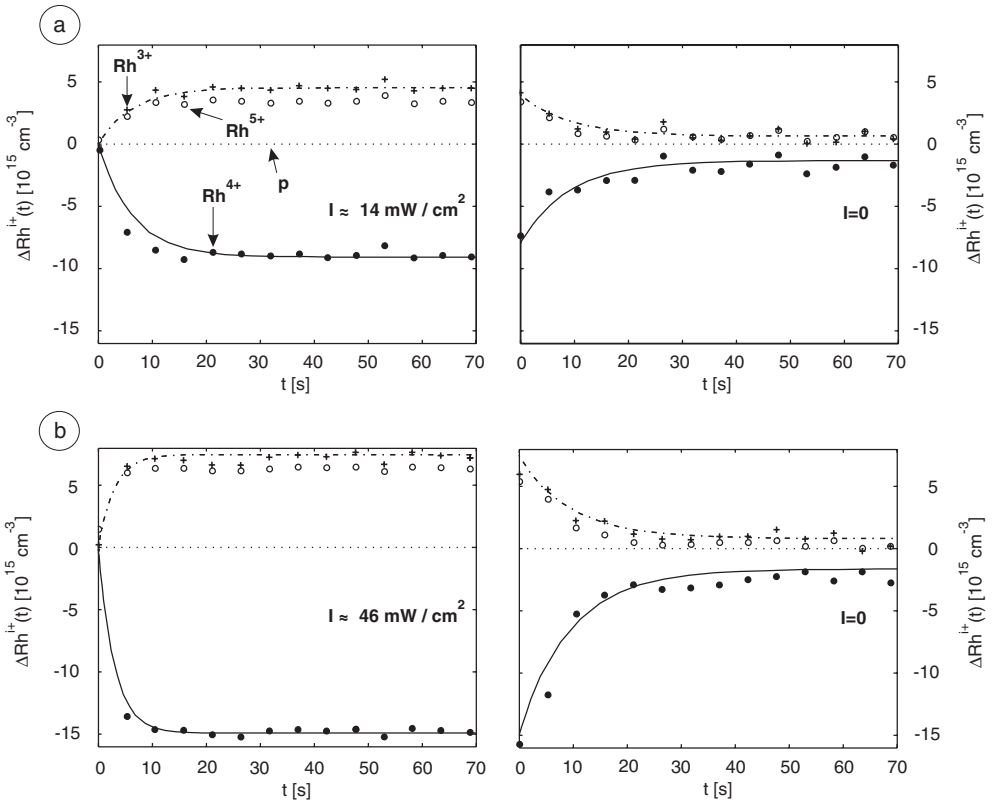

Figure 6. Time dependence (at room temperature) of the light-induced Rh concentration changes after turning light on (left side) and shutting it off (right side) for two light intensities at 633 nm. The smooth curves give the best fits of the numerical solutions of the rate equations (figure 5) to the experimental data. The fitting parameters are listed in table 1.

signals. Previously, data on defect concentrations had to be deduced from a photorefractive determination of the effective charge densities, N_{eff}, see below (equation (4)). As will be shown there, such an analysis gives much more restricted information because it deals with a combined sum of all the densities of the individual Rh^{i+} charge states.

The time dependence of the light-induced concentration changes is governed by the rate equations [10] shown in figure 5; the parameters that are used are explained in the figure. They include the recombination coefficients γ_i, multiplied by the hole density p, and the thermal ionization parameters β_i. The quantities Rh^{i+} denote the respective Rh concentrations, using a more simplified notation than before; I is the pump intensity, given by the number of photons per area and time; q_i is the probability that an absorbed photon will lead to ionization. Figure 6 shows the measured dependences for two pump intensities of 1.96 eV ($\lambda = 633$ nm) pump light and also for cases when the pumplight is switched off. The rather noisy trend of the experimental data is caused by the fact that they had to be taken with probe light (comprising all the energies indicated in the abscissa of figure 3) having intensities as low as possible in order not to influence the investigated absorption changes. This leads to poor signal-to-noise ratios. The full curves are the best fits obtained by numerical integration of the rate equations (figure 5) leading to the parameters in table 1.

The values of the absorption cross-sections $S(Rh^{i+})$, active for the 1.96 eV pump light energy used (figure 4) and the initial Rh^{i+} concentrations (table 1) were entered into these

equations as fixed quantities. The remaining parameters were then varied to obtain the fits indicated in figure 6.

An interesting feature emerges from these data: the light-induced concentration changes do not return to their initial zero values after switching the light off and observing the decay for about 1 min. Apparently this represents a metastable non-equilibrium situation, caused by a slow decay when $I = 0$. This dark decay is triggered by the thermal excitation of holes from Rh^{5+} to the edge of the valence band and their subsequent recombination at Rh^{3+}. At the edge of the band the mobility of the holes is strongly decreased by the fluctuating local potentials, up to the point that complete localization may occur. During photoexcitation ($I \neq 0$), on the other hand, the average mobility might be higher because then the holes are also excited to states within the band. This result is in agreement with anecdotal experimental evidence where a different photorefractive performance of $BaTiO_3$:Rh was observed, depending on the history of the sample and especially its previous illumination.

It is, of course, more desirable that a crystal behaves in a unique way, i.e. that it always returns back to its equilibrium state. This is expected to occur at elevated temperatures, because then the hole mobility increases. We thus tested the dark decay of the crystal at 50 °C. As expected, the concentration changes then relax essentially to zero in the dark. However, since in this situation the recombination processes are faster, the stationary state amplitudes of the changes are smaller than at room temperature. This prevents a reliable evaluation of the data at 50 °C.

The metastable state, reached under dark decay, is the origin of the photochromic effect on which our method of investigation is based. Here we face a conflict of goals: on the one hand, metastability is essential to observe photochromic changes, but at the same time it represents a nonunique situation, because the initial equilibrium Rh^{i+} concentrations differ from those reached after dark decay. This problem, fortunately, does not seriously affect the derived parameters. The maximal concentration changes in figure 6 amount to only about 1% of the total Rh^{i+} concentrations. Since only the latter, and therefore nearly light-independent concentrations, enter into the right sides of the rate equations in figure 5, the derived parameters depend only a little on the fact that the concentration changes do not decay to zero. Indeed all the parameter variations, obtained from fitting to an assumed decay towards $\Delta Rh^{i+} = 0$ during the investigated time span or, alternatively, to the actual final ΔRh^{i+} values, lie within the uncertainty ranges listed in table 1.

When fitting the time dependences in figure 6, it turns out that the ionization probability q_5 has to be assumed to be as high as possible; therefore its value is fixed at 1, meaning that all absorptions lead to ionization. Furthermore, only with q_4 two orders of magnitude smaller than q_5 can an appropriate fit be obtained. The values for γ_3 and γ_4 can be chosen within a wide range, as long as their ratio γ_4/γ_3 remains fixed to about 20. No such choice exists for the values of β_4 and β_5, i.e. they have to lie in the ranges given in table 1. A discussion of these parameters will be given in the next section.

The error ranges listed in table 1 result from a careful assessment of the uncertainties introduced by the following steps:

(1) determination of the Rh^{4+} EPR intensity and its calibration in absolute concentration;
(2) comparison with the light-induced absorption changes;
(3) assuming the validity of the three-valence model, i.e. neglecting the weak transfer of holes to Fe^{i+};
(4) decomposition of total absorption into Gaussian bands
(5) errors connected with fitting the data in figure 6.

4. Discussion of the derived charge transfer parameters

The values of the absorption cross-sections in table 1 correspond roughly to the geometric values expected from the related ionic radii. They thus represent rather strong transitions, typical for charge transfers. This is consistent with the assignment of the corresponding absorption bands to light-induced electron excitations from the oxygen ligands to the central octahedrally coordinated Rh cation. The related oscillator strengths are 0.07 ± 0.03 for Rh^{5+}, 0.05 ± 0.03 for Rh^{4+} and 0.02 ± 0.01 for Rh^{3+}. These values are proportional to the integral over the absorption cross-sections $S(Rh^{i+})$ (figure 4) and are calculated from these using Smakula's equation [17].

The energies of the absorption maxima, 1.9 eV for Rh^{4+} and 1.7 eV for Rh^{5+}, are partly determined by the electronic excitation energies of valence band electrons to the Rh energy levels, $Rh^{3+/4+}$ and $Rh^{4+/5+}$, respectively. These levels lie about 1.0 and 0.7 eV above the valence band edge [11, 18, 19] and can be reached by thermal excitation of valence band electrons. They are thus called thermal levels. The energy differences, 0.9 eV for Rh^{4+} and 1.0 eV for Rh^{5+}, to the optical absorption maxima are expected to be mainly caused by the Stokes' shifts [17], related to the lattice distortion near the defects, occurring under optically induced charge changes. However, in principle, the possibility of optical transitions essentially starting from the valence band states below the band edge cannot be excluded. For such transitions the energy difference between the optical and thermal transition energies is increased, since the latter always begin at the band edge. The linewidths depend both on the lattice distortions and the weighted density of states in the valence band.

It is expected that the thermal ionization from the shallow $Rh^{4+/5+}$ level has a higher probability than from the deep one, $Rh^{3+/4+}$. The derived ratio of the related ionization parameters $\beta_4/\beta_5 \sim 10^{-2}$ is consistent with this.

The ratio of the recombination coefficients, γ_3/γ_4, is related to that of the β_i by the mass action laws corresponding to the rate equations in figure 5. In thermal equilibrium and under $I = 0$ they lead to $\beta_5\gamma_3/\beta_4\gamma_4 = (Rh^{4+})^2/(Rh^{5+}Rh^{3+})$, where the latter quantities are equilibrium Rh concentrations. For the right side of this relation we calculate from table 1 a value of about 0.5. From the experimentally deduced relation $\beta_5 \gg \beta_4$, we thus conclude that $\gamma_4 \gg \gamma_3$, as observed. It should be noted that the above ratio $\beta_5\gamma_3/\beta_4\gamma_4$, being a mass action constant, is independent of the specific specimen from which its value is derived.

The ionization probabilities q_i are mainly determined by the overlap of the optically excited defect states with the valence band Bloch waves; the larger the overlap, the higher the probability for an excited hole to diffuse away. Because of the lower energy distance of the Rh^{5+} level to the valence band, the wavefunction of Rh^{5+} is expected to be more extended than that of Rh^{4+}. This may explain why q_5 is much larger than q_4. It should be noted that q_4, even if small, must not be taken to be zero in order to obtain a fit to the time dependences in figure 6.

Previous investigations [8, 9, 20], aiming at the determination of the parameters in the rate equations of $BaTiO_3$:Rh (figure 5), had to employ experimental methods that provide much less information than the method which we use here. As mentioned before, all the information on the defect densities had to be taken from photorefractive measurements yielding the quantity N_{eff}, which comprises all charge states of Rh (equation (4)). From the present EPR-based studies, on the other hand, we could obtain the individual Rh^{4+} concentrations separately. It is thus not surprising that the previous limited knowledge about the system led to different values of the parameters than those listed in table 1. The most important difference to the present results is the relation $\gamma_3/\gamma_4 > 1$ quoted in these studies [8, 9, 20]. According to the arguments given above, this is not consistent with the fact that $\beta_5 \gg \beta_4$, a condition also found by the other authors. The recombination parameters γ_i obtained by us (table 1), on the other hand, fulfil the required sequence $\gamma_3/\gamma_4 < 1$.

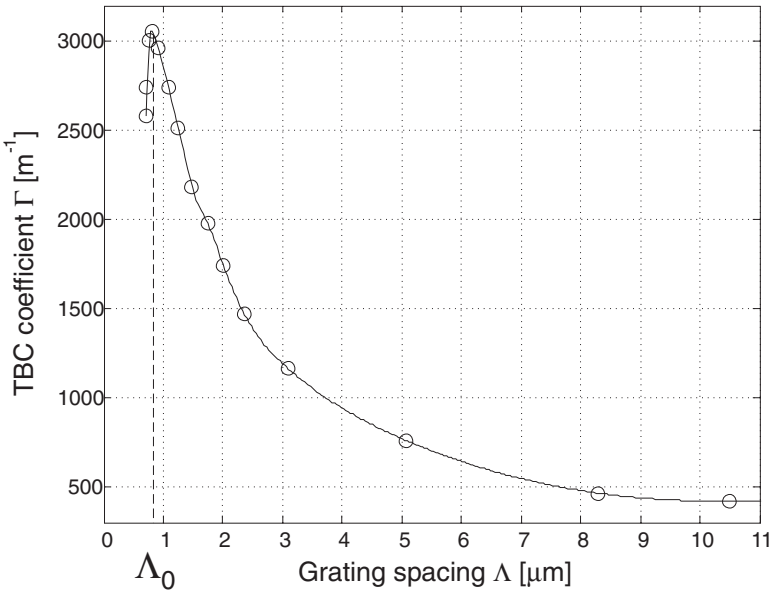

Figure 7. Two-beam coupling gain, which is proportional to the space charge field E_{SC}, measured with the investigated crystal as depending on the grating wavelength Λ.

Furthermore, previously it was not possible to determine the absorption cross-sections S_i and the ionization probabilities q_i, occurring as the products $S_i q_i$ in the rate equations (figure 5), separately. Therefore, the authors of [8, 9, 20] assumed all ionization probabilities q_i to equal 1. Since, however, absorption is not necessarily connected with ionization, this is not justified. It appears that this is the main reason for the absorption cross-sections quoted previously [8, 9, 20] not matching those in table 1 and figure 4.

5. Comparison with photorefractive data

The central quantity in a photorefractive experiment is the space charge field E_{SC} which gives rise to the corresponding refractive index changes via the electrooptic effect. The maximum value of E_{SC}, in turn, is determined by N_{eff}, a measure of the maximal density of charges which can be redistributed under inhomogeneous illumination. For a sinusoidal light pattern leading to an index pattern wavevector k_g, E_{SC} is given by [10]

$$E_{SC} = mkT/e \frac{k_g}{1 + k_g^2/k_o^2} \eta(I) \tag{1}$$

if only diffusion is taken into account as a charge driving mechanism. This assumption is justified for $BaTiO_3$ [21]. The parameter m is the degree of sinusoidal modulation of the intensity. The wavevector $k_o(I)$ is proportional to N_{eff} according to the relation [10]

$$k_o(I) = e^2 N_{eff}/kT\varepsilon_o\varepsilon_r. \tag{2}$$

The saturation factor $\eta(I)$ is related to the ratio between photo- and dark-conductivity:

$$\eta(I) = 1 - \sigma(I = 0)/\sigma(I \neq 0). \tag{3}$$

In the appendix we give the detailed expression for $\eta(I)$ as specified for the three-valence model by Huot *et al* [8]. It is seen there that $\eta(I)$ does not depend on k_g. Therefore, as deduced

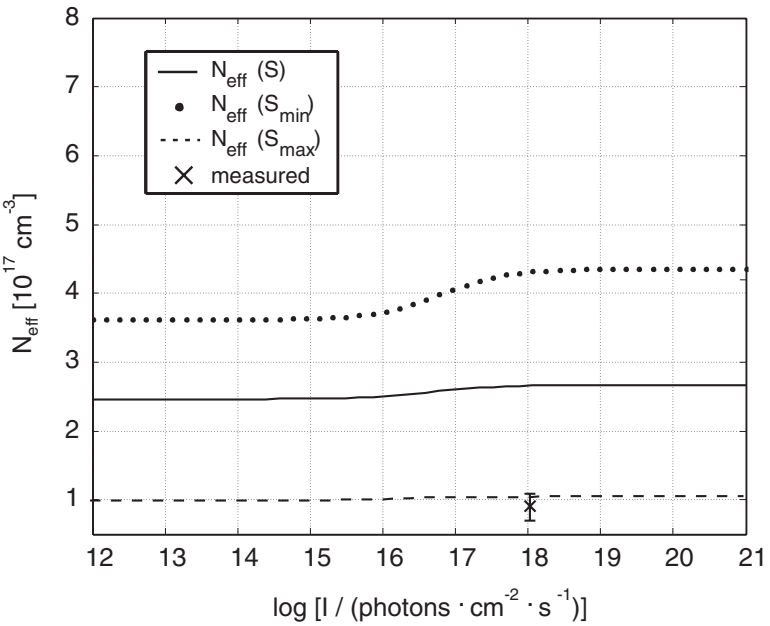

Figure 8. Intensity dependence of the predicted N_{eff} values, as based on the data in table 1. Intensity I is given in (photons cm^{-2} s^{-1}). The parameter uncertainties lead to the shown band of possible N_{eff} values. The experimental N_{eff} is marked by X.

from equation (1), the maximum of E_{SC} occurs for $k_g = k_o$. The available data (figure 7) on $E_{SC}(k_g)$ of the investigated specimen show that this is found at $\Lambda_o = 0.8\ \mu$m, related to k_o by $k_o = 2\pi/\Lambda_o$. In the experiment the vector $\boldsymbol{k}_g$ of the index grating made an angle of 13.5° with the tetragonal axis of the crystal. This leads to an effective value of ε_r being approximately 1020 for this direction ($\varepsilon_\parallel = 168, \varepsilon_\perp = 4300$) [22]. From that, we can derive the value of N_{eff} being $(0.9 \pm 0.2) \times 10^{17}$ cm^{-3}.

This 'experimental' value of N_{eff} will now be compared to the one deduced from the data in table 1, as based on a compact expression for N_{eff}, derived, e.g., by Huot *et al* [8] for the three-valence model:

$$N_{eff}(I) = \mathrm{Rh}_T - \mathrm{Rh}^{4+}(I) - (N_D - N_A)^2/\mathrm{Rh}_T. \tag{4}$$

The quantities N_D and N_A are the donor and acceptor densities, implied to have light-independent valences. They compensate the equilibrium charge densities of Rh^{3+} and Rh^{5+} charges, respectively, which deviate from the replaced Ti^{4+} charges. It is an advantage of our method that the initial concentrations of $Rh^{3+} = N_D$ and $Rh^{5+} = N_A$ are known (table 1). The intensity dependence of $Rh^{4+}(I)$ is calculated from the further parameters in table 1.

Figure 8 shows the calculated intensity dependence of $N_{eff}(I)$, including its range of uncertainty as based on the limits of error given in table 1. It is seen that the experimental value lies in the range predicted by equation (4).

6. Conclusion

The method outlined allows us to distinguish in a qualitative way between which defects photo-induced carriers in a photochromic—and, as a special case, photorefractive—material are

transported under optical excitation. In addition our procedure yields quantitative information on the densities of the defects involved, including those of the background acceptors and donors. These background defects are compensating for the main defects which change their valences under illumination. On this basis the complete set of parameters describing the light-induced charge transfer processes is quantitatively determined. They allow us to predict the photorefractive behaviour of a material. All data are, directly or indirectly, based solely on information obtained by EPR studies of the defects in the respective material. This includes also EPR-silent lattice perturbations. As an example, we analysed in detail the infrared-sensitive photorefractive material $BaTiO_3$ doped with Rh. The identified parameters differ somewhat from those reported in previous publications. This discrepancy can be attributed to the simplifying model assumptions used before and which had to be made in order to cope with the limitations of the experiments used in these studies.

Acknowledgments

We would like to thank Peter Hribek and Robert Eason for useful discussions and their contribution towards measuring two-beam coupling data. Galina Malovichko gave an important hint concerning the interpretation of the light-induced absorption spectra. The help of Wilhelm Koslowski in preparing the manuscript is gratefully acknowledged. Part of this work has been supported by Sonderforschungsbereich 225, funded by DFG.

Appendix

The ratio of the photo- and dark-conductivity, occurring in the expression for $\eta(I)$ (equation (3)), is given by [8]

$$\sigma(I=0)/\sigma(I\neq 0) = (1+S_4q_4I/\beta_4)^{-1}N_{eff,4}/N_{eff} + (1+S_5q_5I/\beta_5)^{-1}N_{eff,5}/N_{eff} \quad \text{(A.1)}$$

with

$$\begin{aligned} &N_{eff,4} + N_{eff,5} = N_{eff} \\ &N_{eff,4}(I) = \mathrm{Rh}^{4+}(I)(\mathrm{Rh}_T + N_D - N_A)/\mathrm{Rh}_T \\ &N_{eff,5}(I) = \mathrm{Rh}^{3+}(I)(\mathrm{Rh}_T - N_D + N_A)/\mathrm{Rh}_T. \end{aligned} \quad \text{(A.2)}$$

The intensity used in the experiment was 330 mW cm^{-2} at a wavelength of 647 nm. Under this condition the quantities (S_iq_iI/β_i) in equation (A.1), as based on table 1, are large compared to 1; since furthermore the factors $N_{eff,i} < 1$ (because of equation (A.2), $\eta(I) \sim 1$. This means that the space charge field was saturated and therefore E_{SC} and also N_{eff} had their maximal possible values in the experiment.

References

[1] Kröse H, Scharfschwerdt R, Mazur A and Schirmer O F 1998 *Appl. Phys.* B **67** 79
[2] Schirmer O F 1999 *Radiat. Eff. Defects Solids* **149** 1
[3] Ruediger A, Schirmer O F, Kadashchuk A and Grabar A 2001 *Trends Opt. Photonics Ser.* **62** 568
[4] Mazur A, Veber C, Schirmer O F, Kuper C and Hesse H 1999 *J. Appl. Phys.* **85** 6751
[5] Ross G W, Hribek P, Eason R W, Garrett M H and Rytz D 1993 *Opt. Commun.* **101** 60
[6] Wechsler B A, Klein M B, Nelson C C and Schwartz R N 1994 *Opt. Lett.* **19** 536
[7] Kaczmarek M and Eason R W 1995 *Opt. Lett.* **20** 1850
[8] Huot N, Jonathan J M C, Pauliat G, Rytz D and Roosen G 1997 *Opt. Commun.* **135** 133
[9] Corner L, Ramos-Garcia R, Petris A and Damzen M J 1997 *Opt. Commun.* **143** 165
[10] Buse K 1997 *Appl. Phys.* B **64** 273

[11] Kröse H, Scharfschwerdt R, Schirmer O F and Hesse H 1995 *Appl. Phys.* B **61** 1
[12] Scharfschwerdt R, Schirmer O F, Hesse H and Rytz D 1999 *Appl. Phys.* B **68** 807
[13] Possenriede E, Jacobs P and Schirmer O F 1992 *J. Phys.: Condens. Matter* **4** 4719
[14] Blazey K W, Schirmer O F, Berlinger W and Müller K A 1975 *Solid State Commun.* **16** 589
[15] Veber C, unpublished
[16] Weil J A, Bolton J R and Wertz J E 1994 *Electron Paramagnetic Resonance* (New York: Wiley) p 498
[17] Fowler W B 1968 *Physics of Color Centers* ed W B Fowler (New York: Academic) p 72
[18] van Stevendaal U, Buse K, Kämper S, Hesse H and Krätzig E 1996 *Appl. Phys.* B **63** 315
[19] Song H, Dou S X, Chi M, Chu Y and Ye P 2000 *Appl. Phys.* B **70** 543
[20] Chi Mingjun, Dou S X, Zhu Yong and Ye Peixian 1999 *Opt. Commun.* **170** 115
[21] Buse K 1997 *Appl. Phys.* B **64** 391
[22] Merz W J 1949 *Phys. Rev.* **76** 1221